Optical constants of a series of amorphous hydrogenated silicon-carbon alloy films: Dependence of optical response on film microstructure and evidence for homogeneous chemical ordering

K. Mui, D. K. Basa,* and F. W. Smith
Department of Physics, The City College of the City University of New York, New York, New York 10031

Reed Corderman
Brookhaven National Laboratory, Upton, New York 11973-5000

(Received 12 November 1986)

The optical constants ($\tilde{n}=n+ik$, $\epsilon_1=n^2-k^2$, $\epsilon_2=2nk$) of a series of amorphous hydrogenated silicon-carbon alloy films (a-$Si_{1-x}C_x$:H) have been determined for photon energies between 1.5 and 4.75 eV. These films have been prepared via the rf glow-discharge decomposition of SiH_4 and C_2H_2. The index of refraction n at 1.5 eV increases smoothly from $n=1.67$ for a-C:H ($x=1$) to $n=3.18$ for a-Si:H ($x=0$), while the optical energy gap E_{opt} reaches a maximum value of 2.68 eV for a carbon fraction of $x=0.68$. The films in this alloy series are proposed to be macroscopically homogeneous, while having a heterogeneous microstructure. Their optical response has been modeled, via the Bruggemann effective-medium approximation (EMA), as arising from three amorphous components: polymeric (a-CH_m, $m\sim 2$), graphitic (a-C), and tetrahedral (a-Si:C:H), and a void component. A Si- and C-centered tetrahedron model developed in the preceding paper has been used to predict the optical response of the amorphous tetrahedral component as a function of its composition. This EMA approach based on four components in the films gives a good description of the observed dependences of ϵ_1 and ϵ_2 on composition and provides a convincing demonstration that the appearance of the amorphous graphitic component in the films limits the attainable value of E_{opt} in this alloy series as the carbon content increases. In addition, the model provides strong evidence that complete chemical ordering with homogeneous dispersion exists within the amorphous tetrahedral (a-Si:C:H) component across the entire alloy series.

I. INTRODUCTION

Amorphous hydrogenated silicon-carbon alloy films (a-$Si_{1-x}C_x$:H) continue to be of considerable current interest both fundamentally in regard to understanding the effect of the local silicon, carbon, and hydrogen bonding configurations on film properties[1-10] and also technologically in regard to their applications as p-type layers in p-i-n a-Si:H photovoltaic devices[11,12] and as potentially useful optical and solar selective coatings.[13] This alloy series spans the range from hydrogenated amorphous Si, a-Si:H ($x=0$), to hydrogenated amorphous C, a-C:H ($x=1$). In a-Si:H, where Si is tetrahedrally coordinated, the hydrogen ($\sim$10—20 at. %) serves to passivate dangling bonds and also to relax the strained a-Si network, thereby contributing to the attainment of a more "ideal" tetrahedrally coordinated Si network with obvious technological applications.[14]

In a-C:H, the situation is more complex due to the fact that C can be bonded in either trigonal (graphitic) or tetrahedral (diamondlike) coordinations. It is clear that the hydrogen ($\sim$30—50 at. %) in a-C:H also serves an important role in passivating dangling bonds and in promoting tetrahedral coordination for the C atoms to which it is bonded.[15-19] These a-C:H films have also been referred to as "diamondlike" due to their high transparency (optical energy gap E_{opt} typically[16] as high as 2.3 eV), high resistivity, and high hardness, and have obvious applications as optical and wear-resistant coatings. In addition, a-C:H can be doped[20] n or p type via the incorporation of P or B atoms, respectively, though not with the same efficiency as has been obtained for a-Si:H.

An outstanding problem for a-C:H has been the preparation of films which are both very hard and optically transparent. The difficulty in achieving this important goal has been due to the relatively small volume fraction ($\sim$0.10—0.15) of graphitically bonded carbon which remains in the films.[19] In order to promote tetrahedral coordination for C in the films, thereby enhancing their diamondlike properties, we have chosen to prepare and characterize the a-$Si_{1-x}C_x$:H films which are the subject of this study.

We have undertaken a careful determination of the optical constants ($\tilde{n}=n+ik$, $\epsilon_1=n^2-k^2$, $\epsilon_2=2nk$) for nine films in the a-$Si_{1-x}C_x$:H alloy series, with compositions given by $x=0$, 0.16, 0.28, 0.38, 0.57, 0.68, 0.84, 0.96, and 1.0. These alloy films have been prepared via the rf glow-discharge decomposition of SiH_4 and C_2H_2. In addition to determining n and k from measurements of film reflectances (air and substrate sides) and transmittance in the range of photon energies from 1.5 to 4.75 eV, measurements of film density, composition (via a scanning Auger microprobe), and hydrogen content (via infrared absorption) have also been undertaken for these films. We

note that in a previous work[10] we have presented results for the optical constants, and their evolution with annealing, of a C-rich alloy film with x approximately equal to 0.8.

We have proposed a microstructural model for these macroscopically homogeneous but microscopically heterogeneous composite a-$Si_{1-x}C_x$:H alloy films in which the films are considered to be composed of amorphous polymeric (a-CH_m, $m \sim 2$), amorphous graphitic (a-C), amorphous tetrahedral (a-Si:C:H), and void components, each with its own dielectric response. For the amorphous tetrahedral component, a Si- and C-centered tetrahedron model has been developed[21] (see preceding paper) in order to predict the optical constants of this component as a function of its Si/C ratio. For this purpose, we have followed the approach of Aspnes and Theeten[22] [developed for $Si_{1-x}(SiO_2)_x$ and $Si_{1-x}(Si_3N_4)_x$ mixtures] and have used a scaling approach to obtain values for ϵ_1 and ϵ_2 for each distinct Si- and C-centered tetrahedron from our results for a-Si:H. Details of this model are given in the preceding paper and are summarized below.

By using our experimental results for ϵ_1, ϵ_2, and film density ρ in conjunction with the effective medium approximation (EMA),[23] we have determined the volume fractions of the four proposed components in the a-$Si_{1-x}C_x$:H films as functions of the carbon fraction x. Briefly, as the carbon fraction x increases, an amorphous graphitic component first appears at $x=0.54$ and then increases smoothly to 17% of the film volume for $x=1$ (a-C:H). The amorphous polymeric component also first makes a significant appearance at $x=0.54$ and then increases smoothly to 67% of the film volume for $x=1$. The amorphous tetrahedral component decreases smoothly from 100% at $x=0$ (a-Si:H) to 16% of the film volume at $x=1$. In addition, the void volume fraction reaches a maximum value of 26% at an intermediate composition, $x=0.38$, and is essentially zero for $x=0$ and $x=1$.

A striking feature of the a-$Si_{1-x}C_x$:H alloy series is the observation[1,5,24] of a maximum in E_{opt} in the range 2.6–2.8 eV at a composition typically between $x=0.6$ and 0.7. We have observed a similar maximum in the dependence of E_{opt} on x and, from the results of our optical constants measurements (as analyzed via the EMA), have been able to show that the increase of E_{opt} as Si is added to a-C:H arises from the conversion of trigonally bonded carbon to a tetrahedral form, while the increase of E_{opt} as C is added to a-Si:H is due to the replacement of Si—Si bonds by stronger Si—C bonds. The maximum in E_{opt} observed for a-$Si_{1-x}C_x$:H can thus be directly related to the growing influence of trigonally bonded (graphitic) carbon atoms as the carbon content is increased.

An important issue for a-$Si_{1-x}C_x$:H films is the nature of the bonding of the Si and C atoms in the amorphous tetrahedral component. In particular, the question of whether chemical ordering occurs in this component remains open, with evidence existing both for and against.[3,4,8] Complete chemical ordering, which corresponds to the maximum possible number of Si—C bonds actually present in the films [with no Si—Si bonds for $x \geq 0.5$ (C-rich) and no C—C bonds for $x \leq 0.5$ (Si-rich)], is unlikely. From our EMA analysis of the measured optical constants, we have, however, observed a tendency for homogeneous chemical ordering, without phase separation, for the amorphous tetrahedral component across the entire alloy series. It is clear from our results that optical constants measurements are a sensitive probe both of film microstructure and of chemical ordering in the a-$Si_{1-x}C_x$:H alloy series.

II. EXPERIMENT

The a-$Si_{1-x}C_x$:H alloy films studied here were prepared in an rf glow-discharge system (Fig. 1). In this system, rf power at 13.56 MHz was capacitively coupled to the powdered electrode. The sample substrates, polished clear fused quartz for optical constants measurements, oxygen-free high-conductivity (OFHC) copper for density and composition measurements, and intrinsic Si for infrared studies (resistivity of 2500 Ω cm, polished both sides), were mounted on the grounded unpowered electrode. The unpowered sample electrode consisted of a heatable copper block with a recessed thermocouple placed just below the sample substrates for temperature measurement. The two electrodes were separated by 2 in., had diameters of 3 in., and were shielded from the plasma except for their front surfaces.

Acetylene (C_2H_2, 99.6% purity, Linde) and silane (SiH_4, diluted to 10.2% in Ar, Linde) were mixed to the desired $[C_2H_2]/[SiH_4]$ ratios in a separate gas handling system and delivered to the top of the discharge chamber via an electronic mass flow controller. The discharge chamber, which could be pumped to the low 10^{-7}-Torr range via a diffusion pump prior to deposition, was exhausted via a mechanical pump during the glow-discharge process. Exhaust gases from the discharge itself were passed through an oven and then through a NaOH bubbler for neutralization.

Typical deposition parameters were a starting pressure of 0.15 Torr, flow rates of typically 1 sccm (cubic centim-

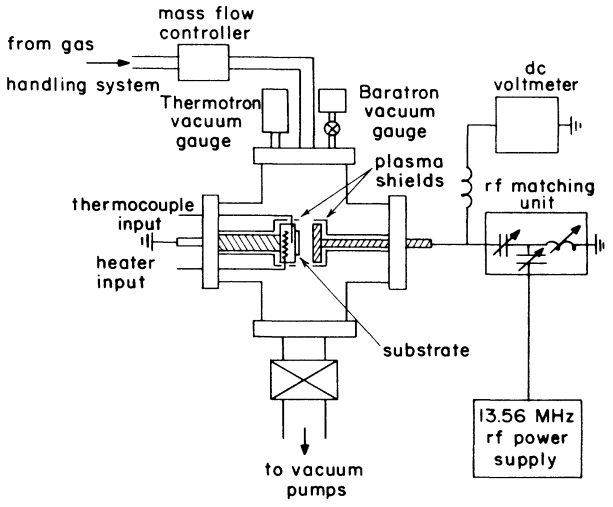

FIG. 1. Schematic of rf glow discharge deposition system.

TABLE I. Compositions, densities, and energy gaps of a-$Si_{1-x}C_x$:H films.

$f(C_2H_2)$[a]	x[b]	x(EMA)[c]	ρ (g/cm^3)[d]	E_{opt} (eV)[e]	B_1[e]	B_T[f] (cm eV)$^{1/2}$	E_{04} (eV)[g]
1.00	1.00±0.02	1.00±0.02	1.36±0.03	2.24±0.04	1.63	273	2.81
0.91	0.96±0.03	0.96±0.01	1.36±0.03	2.36±0.05	1.63	272	2.92
0.80	0.84±0.06	0.83±0.03	1.45±0.05	2.38±0.04	1.59	268	3.00
0.72	0.68±0.05	0.68±0.04	1.58±0.02	2.68±0.07	2.34	364	2.98
0.60	0.57±0.08	0.54±0.04	1.69±0.02	2.65±0.05	3.27	464	2.78
0.50	0.38±0.06	0.38±0.01	1.86±0.04	2.49±0.05	3.98	532	2.60
0.35		0.28±0.01	1.93±0.03	2.26±0.05	5.65	708	2.25
0.20	0.07±0.06	0.16±0.01	2.00±0.04	2.21±0.05	7.60	859	2.00
0.00	0.00±0.02	0.00	2.07±0.09	1.8 ±0.20	5.5	700	1.75

[a]Fraction of C_2H_2 in glow discharge.
[b]Carbon fractional content of film determined from scanning Auger microprobe.
[c]Carbon fractional content of film determined using the effective medium approximation (EMA), see text.
[d]Film density.
[e]Optical energy-gap parameters determined from $\epsilon_2(E)=B_1(E-E_{opt})^2/E^2$.
[f]B_T determined from $(\alpha E)^{1/2}=B_T(E-E_{opt})$.
[g]E_{04} is the energy at which the absorption coefficient α is equal to 10^4 cm^{-1}.

eters per minute at standard temperature and pressure), discharge power of 15 W, substrate temperature T_s of 250 °C, and deposition rates from 0.3 to 2.7 Å/sec, increasing as the C_2H_2 percentage in the discharge mixture increased. The substrates were given an Ar glow-discharge cleaning (0.15 Torr, 15 W, $T_s=250$ °C, 3 min) *in situ* just prior to deposition of the alloy films. Film thicknesses were in the range from 450 to 4800 Å, and were determined optically (see below). Nine different alloy compositions were investigated, as listed in Table I. Film compositions have been determined from Auger spectra which were obtained using a Perkin Elmer Corp. Physical Electronics Division PHI 600 Scanning Auger Microprobe. All Auger spectra were measured with a primary electron beam energy of 3 keV, an electron beam diameter of 400 nm, and an electron beam current, measured at the sample, of ~35 nA (except for the film with a carbon content of 0.96, for which the electron beam current was reduced to 16 nA). The depth profile of each film was obtained by sputtering using a 3-keV Ar^+-ion beam. The vacuum chamber pressure was 1.0×10^{-8} Torr during sputtering.

Film density measurements were undertaken using the flotation method in solutions of $ZnBr_2$ in H_2O. These films had been removed by dissolving the OFHC Cu substrates in concentrated ferric chloride. Estimates of the hydrogen contents in the a-C:H and a-Si:H films were obtained from infrared (ir) absorption studies which were carried out on both IBM IR95 and Digilab 60 FTIR (Fourier-transform ir) spectrophotometers, in the range 450—4000 cm^{-1}.

For the determination of the real and imaginary parts of the index of refraction (n and k, respectively) and of the dielectric constant ($\epsilon_1=n^2-k^2$ and $\epsilon_2=2nk$, respectively), measurements of the film reflectances from both the air R_a and substrate R_s sides of the film as well as the film transmittance T were undertaken. These measurements were carried out on a Perkin Elmer Lambda 3 spectrophotometer in the range 2550—8950 Å. A specular reflectance accessory calibrated using a National Bureau of Standards (NBS) SRM 2023 specular reflectance standard was employed for the determinations of R_a and R_s.

III. ANALYSIS AND RESULTS

A. Film compositions

The Si and C contents of the films prepared on Cu substrates have been determined directly by means of a scanning Auger microprobe (SAM). Depth profiles of Si, C, and Cu were obtained throughout the films and into the substrate for eight of the nine alloy films studied. The atomic fractional concentrations, F_x, of Si, C, and Cu were calculated using Eq. (1),

$$F_x=(I_x/S_x)/\sum_n (I_x/S_x)\ , \tag{1}$$

where I_x is the Auger peak-to-peak intensity after a five-point differentiation of data collected in a 20-eV electron kinetic energy region about the peak energy for each element, S_x is the Auger sensitivity factor for each element at 3 keV, and n sums over the three elements C, Si, and Cu. Standard values for the Auger sensitivity factors were used.[25] After subtracting the baseline atomic concentrations of Si and C observed in the substrates from the values observed in the films, the resulting values, f(Si) and f(C), were normalized to their sum to obtain the Si and C fractional concentrations. The results for the fractional carbon concentrations in these a-$Si_{1-x}C_x$:H alloys, $x=f(C)/[f(Si)+f(C)]$, are listed in Table I, along with the estimated uncertainties. We note that for the two Si-rich samples for which SAM studies were undertaken, with $x=0.07$ and 0.38, evidence for a buildup of carbon at the film-substrate interface was observed from the depth profile. This carbon enrichment of the film-substrate interface could also be detected from the optical measurements (see below). In addition, excess carbon was typically observed on the film surfaces which had been exposed to air. Using the optically measured thickness for each film and a sputtering time for each film measured

from the surface to where either the C or Si content has decreased to 50% of its average original value, sputtering rates for the various a-$Si_{1-x}C_x$:H films have been calculated. No definitive trend in sputtering rate with increasing C concentration (decreasing Si concentration) is observed. The average sputtering rate, excluding the 100% a-Si:H and a-C:H films, is calculated to be 9.2 Å/s.

Also listed in Table I are carbon fractional concentrations, x(EMA), which were determined by means of the effective medium approximation, in which the film was considered to be composed of amorphous polymeric, graphitic, tetrahedral, and void components. Details of how these values for x(EMA) were obtained will be presented below.

B. Hydrogen content and film density

Estimates of the bonded hydrogen contents of some of these films have been obtained from the integrated absorbances of the carbon-hydrogen and silicon-hydrogen infrared stretching modes. For the a-C:H film prepared from 100% C_2H_2, C—H_n modes were observed at 2865, 2930, and 2960 cm^{-1}, with some weak absorption extending up 3050 cm^{-1}. Using a cross section for these modes of $(1.35\pm0.35)\times10^{21}$ cm^{-2}, which is an average of the results of 1.0×10^{21} and 1.7×10^{21} cm^{-2} given by Fujimoto *et al.*[26] and Nakazawa *et al.*,[27] respectively, a hydrogen atomic concentration of $(7.4\pm1.9)\times10^{22}$ cm^{-3} and a hydrogen atomic percentage of (54 ± 14) at. % were obtained. The H atomic percentage is based on a measured density of 1.36 g/cm^3 for this a-C:H film (see below). The ratio of C—H bonds to C atoms in this film, [C—H/C], was found to be 7.4×10^{22} $cm^{-3}/6.2\times10^{22}$ $cm^{-3}=1.2$. In addition to the C—H_n stretching modes, C—H_n bending modes were observed at 1390 and 1460 cm^{-1}.

For a film prepared from 56% C_2H_2 and 44% SiH_4, in addition to C—H_n stretching modes in the range 2865—2960 cm^{-1} and bending modes at 1405 and 1460 cm^{-1}, bending modes at 1350 (C—H_n) and 1255 cm^{-1} (SiC—H_3) were observed. The silicon-hydrogen stretching mode at 2095 cm^{-1} (with a width at half maximum of 90 cm^{-1}) was observed, along with the SiC—H_n wagging mode near 990 cm^{-1} and the Si—C stretching mode at 775 cm^{-1}. The Si—C stretching mode was the dominant absorption feature in this spectrum. Integrated absorbances of the C—H and Si—H stretching modes (using an Si-H cross section[28] of 1.4×10^{20} cm^{-2}) yielded 3.4 and 1.0×10^{22} hydrogen atoms/cm^3, respectively, in these bonds, for a total hydrogen atomic percentage of 46 at. %. To determine the latter we have assumed equal densities of carbon and silicon atoms in the film and a film density of 1.78 g/cm^3. The [C—H/C] and [Si—H/Si] ratios for this film were found to be 1.3 and 0.4, respectively.

For the film prepared from 100% SiH_4, Si—H stretch modes at 2000 and 2090 cm^{-1}, weak bending modes at 840 and 900 cm^{-1}, and the wagging mode at 640 cm^{-1} were observed. From the stretching modes, a hydrogen concentration of 3.5×10^{21} cm^{-3} was obtained, yielding 7.6 at. % hydrogen for a measured film density of 2.07 g/cm^3. The [Si—H]/[Si] ratio for this film was found to be 0.08.

The measured densities of these films are listed in Table I. Film density increases smoothly from a value of 1.36 g/cm^3 for a-C:H to 2.07 g/cm^3 for a-Si:H, with the most rapid increase in density occurring as the Si fractional content increases in the range from 0.2 to 0.6.

C. Optical constants

For the determination of values of n, k, and d (the film thickness) from the optical measurements, we have employed a computer fitting procedure based on the theory[29] for the exact amplitudes of the reflected and transmitted waves in the films, including the effects of interference. Interference effects in the substrates have, however, been averaged out of the analysis since in practice these canceled out. The procedure used for determining the correct film thickness d, and simultaneously n and k, is similar to that outlined by Nagendra and Thutupalli.[30] We have, however, not used the expressions given by Nagendra and Thutupalli for R_a, R_s, and T since they have not included reflections occurring from the back surface of the substrate. This procedure employs the two-dimensional Newton-Raphson technique for the determination of the sets of values of n and k which, for a given d and wavelength λ, produce exactly two of the measured quantities R_a, R_s, and T. The main advantage of the Newton-Raphson technique is its rapid convergence. For a given d and λ, there can exist multiple sets of solutions for n and k, and choosing the correct values of n, k, and d involves an examination of the variation of n and k with λ for a given d. When the best thickness d is employed, smooth, continuous curves for n and k as functions of λ will in general be obtained.

As a further check, the values of d determined above were used in a previously employed fitting procedure[10] which makes use simultaneously of all three measured quantities, R_a, R_s, and T. Good agreement has been obtained for n and k from these two procedures. For several alloy concentrations on the Si-rich end of the alloy series (where n and k vary appreciably with photon energy), it was necessary to deposit films of differing thicknesses so that smooth values of n and k could be obtained over the entire photon energy range from 1.5 to 4.75 eV. Typical uncertainties in d were from $\pm2\%$ to $\pm5\%$, while for n and k they were ±0.04 and up to ±0.02, respectively.

The previously mentioned carbon enrichment of the film-substrate interface was also apparent from these optical measurements for the Si-rich films with C fractions of 0.07, 0.28, and 0.38. For these films, measured values of R_a yielded values for n and k which were not consistent with those determined from R_s for high photon energies (greater than 4 eV). Values of R_s were instead consistent with lower n and k values for these films at the film-substrate interface, which would be the case if the region of the film next to the interface had a higher C content than the bulk of the film.

Results for n and k for the nine films studied are presented in Figs. 2 and 3 as functions of photon energy E. Both n and k show a significant variation with concentration, with both increasing from a-C:H to a-Si:H.

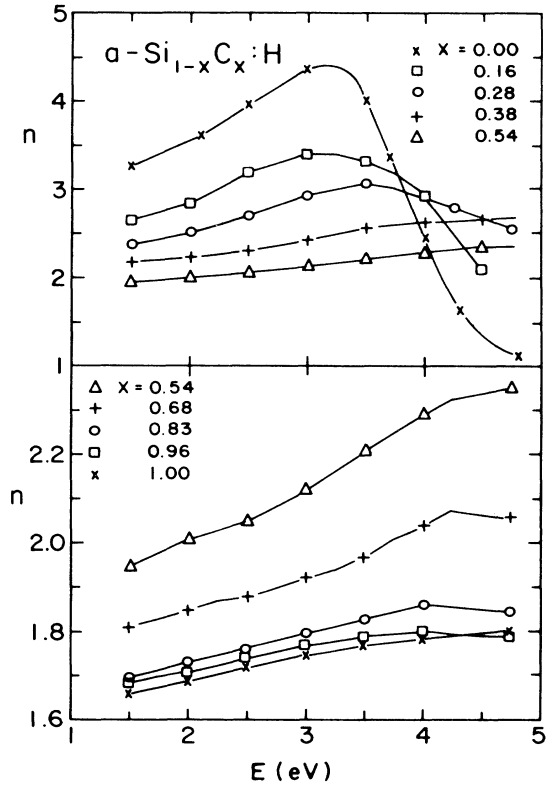

FIG. 2. Index of refraction n vs photon energy for nine a-$Si_{1-x}C_x$:H films. Carbon contents as listed have been determined via the EMA (see text and Table I).

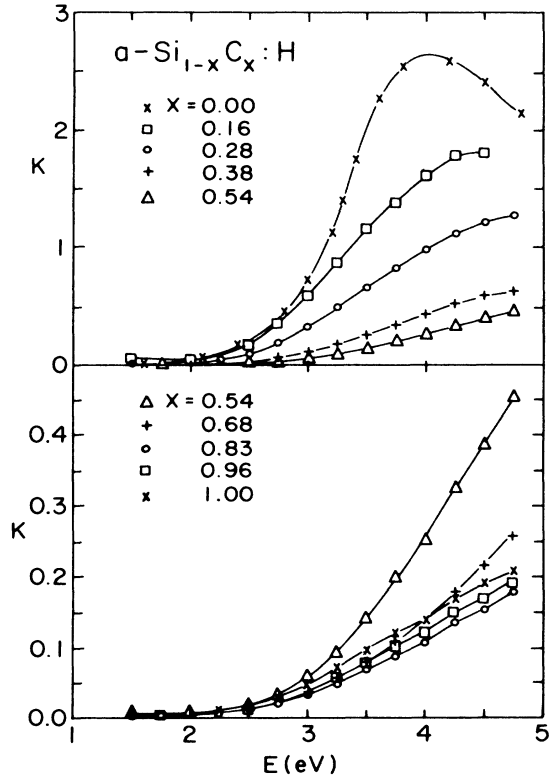

FIG. 3. Extinction coefficient k vs photon energy for nine a-$Si_{1-x}C_x$:H films. Carbon contents as listed have been determined via the EMA (see text and Table I).

For this reason, n and k values for the C-rich and Si-rich films are shown separately. ϵ_1 and ϵ_2 as functions of photon energy are shown in Figs. 4 and 5. Our results for k (and $\epsilon_2 = 2nk$) show an initial small *decrease* as Si is added to a-C:H, signaling a decrease in film absorption. This decrease is also apparent in Fig. 6 where the absorption coefficient α is presented for all nine films as a function of energy.

D. Optical energy gap

We have used the Tauc plot[31] of $E(\epsilon_2)^{1/2}$ versus E to obtain the optical energy gaps E_{opt}, defined by $\epsilon_2(E) = B_1(E - E_{\text{opt}})^2/E^2$, for these films. Values for E_{opt} and B_1 (dimensionless) are listed in Table I. E_{opt} increases from 2.24 eV for a-C:H ($x = 1$) to a value of 2.68 eV for $x = 0.68$, before decreasing to a value of 1.8 eV for a-Si:H ($x = 0$). The slope B_1, which is inversely proportional to the width of the tail state band, first shows a slight decrease (1.63 to 1.59) as Si is added to a-C:H before increasing to a value of 5.5 for a-Si:H.

Other workers[1,2,5,24] who measure only film absorption typically employ the Tauc plot in the form $(\alpha E)^{1/2} = B_T(E - E_{\text{opt}})$. We have used our results for the absorption coefficient $\alpha = 4\pi k/\lambda$ to test this expression and have found that it gives essentially the same values for E_{opt} as the more correct expression which makes use of $E(\epsilon_2)^{1/2}$ and which explicitly takes into account the energy dependence of the index of refraction n. The constant B_T in the expression involving α is related to the corresponding constant B_1 by $B_T = (B_1/\bar{n}\hbar c)^{1/2}$ where $\bar{n}$ is the average index of refraction in the energy region where the Tauc plot is applicable (typically 3 to 5 eV for carbon-rich samples and 2.5 to 3.5 eV for silicon-rich samples). For comparison with the results of other workers, our results for B_T obtained from the $(\alpha E)^{1/2}$ plot are also included in Table I. Values for B_T calculated directly from B_1 and $\bar{n}$ using the above expression are systematically lower by 20% to 100% than those listed in Table I. Also included in Table I are values for E_{04}, the energy at which the absorption coefficient α is equal to 10^4 cm^{-1}.

E. Effective-medium approximation

An important goal of this research is to obtain information concerning the types of bonding of carbon, silicon, and hydrogen atoms in these films from the measured optical constants. For this purpose we have used the Bruggemann effective-medium approximation (EMA) for composite heterogeneous media.[23] For the EMA to be valid, the scale of the heterogeneity in the film (i.e., the dimensions of the distinct regions corresponding to the various components) must be much smaller than the wavelength of light in the medium, yet large enough so that the individual components have "bulklike" dielectric properties. The use of the EMA has previously been shown to be

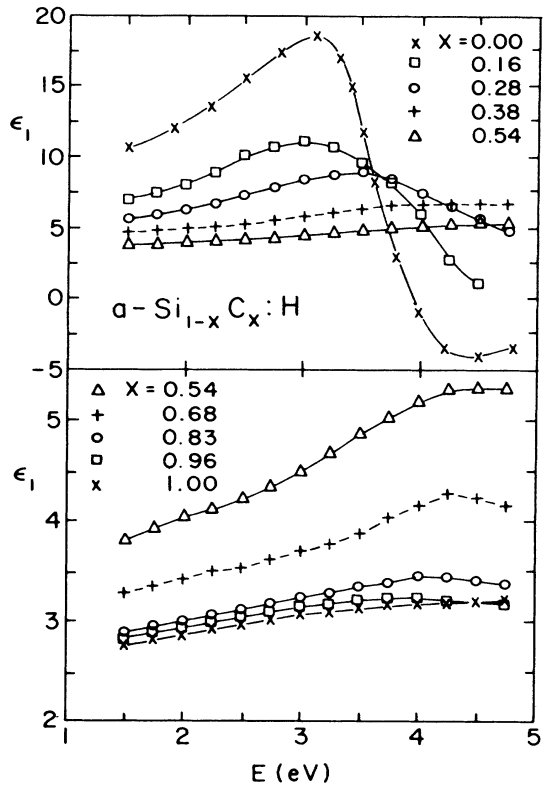

FIG. 4. Real part ϵ_1 of the dielectric constant vs photon energy for nine a-$Si_{1-x}C_x$:H films. Carbon contents as listed have been determined via the EMA (see text and Table I).

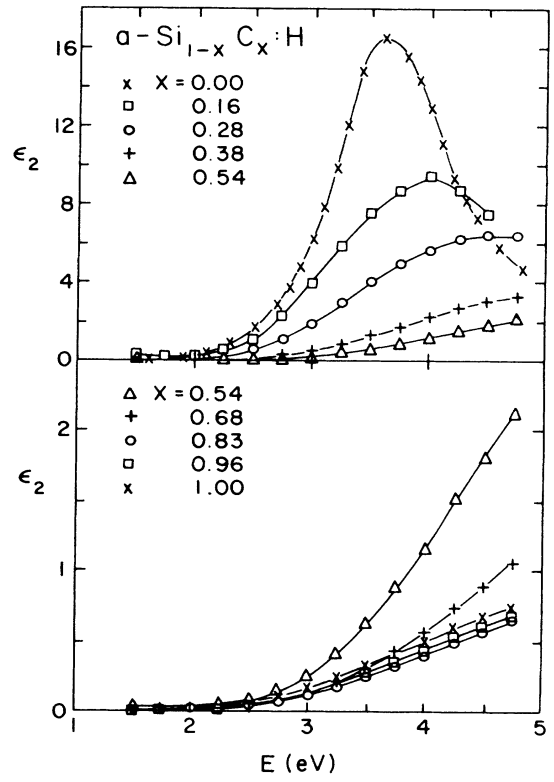

FIG. 5. Imaginary part ϵ_2 of the dielectric constant vs photon energy for nine a-$Si_{1-x}C_x$:H films. Carbon contents as listed have been determined via the EMA (see text and Table I).

applicable both to hydrogenated amorphous carbon films (a-C:H) (Ref. 19) and also to Si-SiO_2 and Si-Si_3N_4 mixtures,[22] and its extension to these a-$Si_{1-x}C_x$:H alloy films is a natural one. The EMA expression for ϵ, the complex dielectric function of the composite medium, is given by

$$\sum_i v_i \frac{\epsilon_i - \epsilon}{\epsilon_i + 2\epsilon} = 0 \,, \qquad \sum_i v_i = 1 \,, \tag{2}$$

where v_i and ϵ_i are the volume fraction and complex dielectric function of component i, respectively.

For a-C:H, a successful representation[19] of the measured ϵ was based on the existence of four components in the films: amorphous polymeric, amorphous graphitic, amorphous diamondlike, and void. The amorphous polymeric component represented that fraction of the carbon in the film which is hydrogenated, C—H_m, i.e., bonded in configurations with $m=2$ or 3. The amorphous graphitic component represented the threefold (trigonally) coordinated carbon, and the amorphous diamondlike component represented the fourfold (tetrahedrally) coordinated carbon. The manner in which the volume fractions of these four components varied as the film was annealed was the subject of a previous investigation.[19] For Si-SiO_2 and Si-Si_3N_4 mixtures, the fundamental units which determine

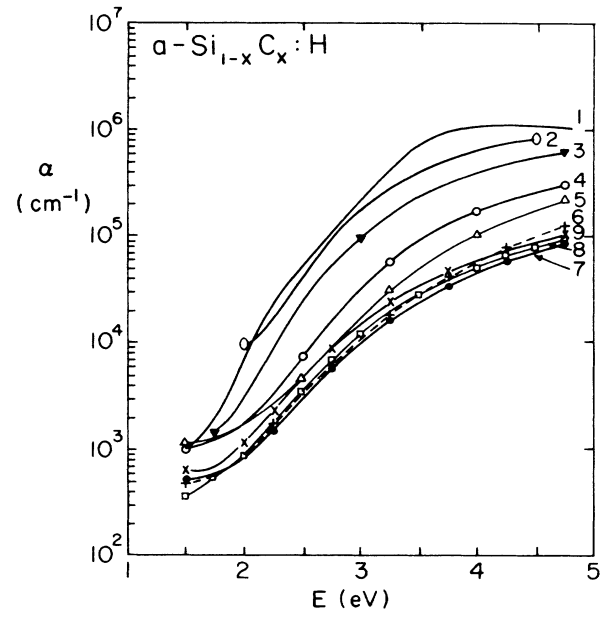

FIG. 6. Absorption coefficient α vs photon energy for nine a-$Si_{1-x}C_x$:H films. Carbon contents 1: $x=0.00$; 2: $x=0.16$; 3: $x=0.28$; 4: $x=0.38$; 5: $x=0.54$; 6: $x=0.68$; 7: $x=0.83$; 8: $x=0.96$; 9: $x=1.00$.

the optical response of the films were taken to be Si-centered tetrahedra,[32] i.e., Si-Si$_{4-v}$N$_v$ and Si-Si$_{4-v}$O$_v$ tetrahedra ($v=0$ to 4), respectively. This approach was found to be successful in reproducing measured dielectric function data for these mixtures.[22]

For the a-Si$_{1-x}$C$_x$:H alloy films under study here, we propose that the following components will determine the dielectric response: amorphous polymeric (a-CH$_m$, $m\sim 2$, with volume fraction v_{ap}), amorphous graphitic (a-C, v_{ag}), amorphous tetrahedral (a-Si:C:H, v_{at}) and void (v_v). This approach is a natural extension of the one previously used[19] for a-C:H with the addition that the amorphous tetrahedral component now contains both Si and C, along with some hydrogen. We wish to emphasize that these a-Si$_{1-x}$C$_x$:H films, although assumed to be heterogeneous on a microscopic level, are nevertheless macroscopically homogeneous.

In order to apply the EMA expressed by Eq. (2) to our measured ϵ_1 and ϵ_2 spectra so that the volume fractions v_i of the proposed components can be obtained, we first need the ϵ_i spectra for the individual components. For the amorphous polymeric component we use the same ϵ_1 and ϵ_2 as employed previously for a-C:H, based on smoothed data[33] for polyethylene with a density of 0.92 g/cm^3. For the amorphous graphitic component we have chosen to use our previously measured ϵ_1 and ϵ_2 spectra[19] for an a-C:H film annealed at 500 °C, with a measured density of 1.47 g/cm^3. The dielectric response of this annealed a-C:H film is believed to more accurately reflect the localized nature of the graphitic π-like electrons than did the evaporated C film previously used.

The dielectric response of the amorphous tetrahedral component presents more of a challenge as there exist no measured spectra for completely tetrahedrally-coordinated a-Si:C:H. We have therefore developed in the preceding paper[21] a Si- and C-centered tetrahedron model in order to calculate the ϵ_1 and ϵ_2 spectra for the a-Si:C:H tetrahedral component as a function of its composition. These ϵ_1 and ϵ_2 spectra have been obtained by scaling from our ϵ_1 and ϵ_2 data for a-Si:H (this work), and, as a result, the dielectric response of the amorphous tetrahedral component can be considered to reflect the contribution of approximately 10 at. % hydrogen.

An additional aspect of the problem of obtaining appropriate ϵ_1 and ϵ_2 spectra for the amorphous tetrahedral component involves the issue of whether or not chemical ordering occurs in the bonding between C and Si atoms. The cases of no chemical ordering, homogeneous chemical ordering, and phase-separated chemical ordering lead to significantly different ϵ_1 and ϵ_2 spectra for the amorphous tetrahedral component,[21] particularly for compositions near $x=0.5$. We will use our measured ϵ_1 and ϵ_2 spectra in the EMA not only for the determination of the v_i, but also to provide information on whether or not the Si and C atoms in the amorphous tetrahedral component[21] have a tendency to be chemically ordered.

Our experimental results for ϵ_1 and ϵ_2, along with the ϵ_i spectra for the proposed components specified as described above, have been used in Eq. (2) for the EMA in order to determine the volume fractions v_i (i.e., v_{ag}, v_{ap}, v_{at}, and v_v) of the four components present in these a-Si$_{1-x}$C$_x$:H films, as functions of film composition x. A least mean-square fitting procedure, which involved minimizing not only the real and imaginary parts of Eq. (2), but also the difference between the measured film density (Table I) and the calculated film density (equal to $\sum_i v_i\rho_i$), where the ρ_i are the densities of the individual components), has been employed to obtain the best values for the v_i. As for the case of a-C:H,[19] the measured film densities have been crucial in setting constraints on the possible v_i of the various components. In this fitting procedure, the film stoichiometry x as well as the volume fractions v_i of the components have been allowed to vary in order to obtain a best fit.

In addition to determining the film stoichiometry x and the volume fractions v_i the fitting procedure has also enabled us to test for the existence or absence of chemical ordering in the amorphous tetrahedral component for these a-Si$_{1-x}$C$_x$:H films. We illustrate the effect of chemical ordering on ϵ_1 and ϵ_2 for the film which, according to the Auger measurement, contained a carbon fraction of 0.38. Assuming complete chemical ordering with homogeneous dispersion in the amorphous tetrahedral component, the best fit to the measured ϵ_1 and ϵ_2 was obtained for a carbon fraction of 0.38 ± 0.01, in excellent agreement with the Auger result. This fit to the experimental ϵ_1 and ϵ_2 is shown in Figs. 7 and 8, along with the best fits to the data under the assumptions of complete chemical ordering with phase separation and of no chemical ordering. It is clear from Figs. 7 and 8 that complete chemical ordering with homogeneous dispersion gives the best fit to the data for this sample.

The results obtained from the EMA for the volume fractions of the various components present in these a-Si$_{1-x}$C$_x$:H films are listed in Table II and plotted in Fig. 9 as functions of film composition. For all the alloy sam-

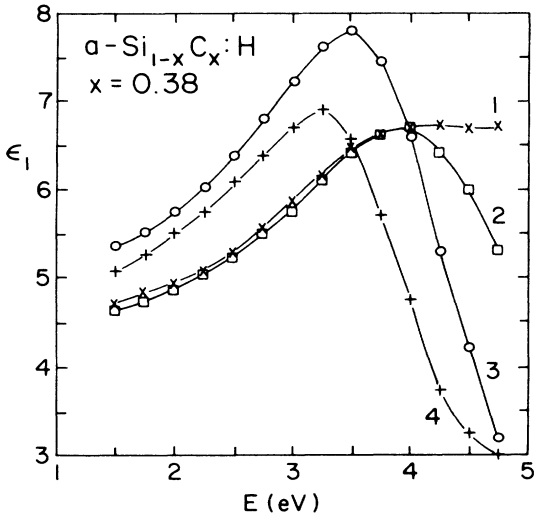

FIG. 7. ϵ_1 vs photon energy for a-Si$_{0.62}$C$_{0.38}$:H. Curve 1: experimental points; curve 2: complete chemical ordering with homogeneous dispersion; curve 3: no chemical ordering; curve 4: complete chemical ordering with phase separation.

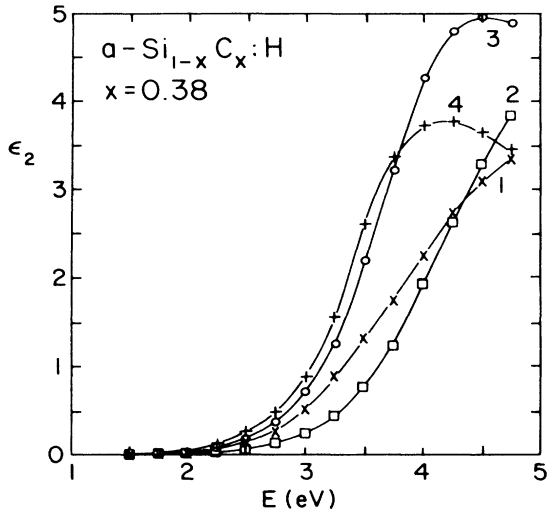

FIG. 8. ϵ_2 vs photon energy for a-$Si_{0.62}C_{0.38}$:H. See Fig. 8 for labeling of curves.

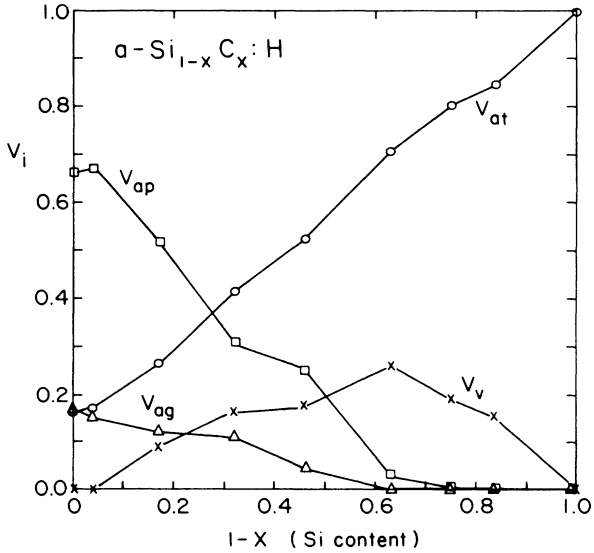

FIG. 9. Volume fractions of the various components of the a-$Si_{1-x}C_x$:H films as functions of $1-x$ (Si content). v_{at} represents amorphous tetrahedral, v_{ap} represents amorphous polymeric, v_{ag} represents amorphous graphitic, and v_v represents void.

ples studied, the best possible fits to the data using the EMA favored complete chemical ordering with homogeneous dispersion over no chemical ordering. Also listed in Table II are the EMA results for x(EMA), the carbon fraction in the film which gave the best fit in the EMA, and x_{at}, the corresponding carbon function in the amorphous tetrahedral component. We note that x_{at} is less than x(EMA) for films in which a fraction of the carbon atoms are in the amorphous polymeric and graphitic components.

Beginning with a-C:H ($x=1.0$), the major component in the film is found to be the amorphous polymeric one (67%), with significant amounts of amorphous graphitic (17%) and amorphous tetrahedral or diamondlike (16%) components also found to be present. These results are quite consistent with previous results[19] obtained for an a-C:H film prepared via a dc glow discharge technique, where corresponding percentages of 75%, 11%, and 14% for these three components were obtained. As Si is added to the a-C:H film, it can be seen from Table II and Fig. 9 that the amorphous polymeric and amorphous graphitic components gradually decrease essentially to zero at a Si fractional content of 0.62 ($x=0.38$). At the same time, the amorphous tetrahedral component increases, reaching 100% for $x=0$ (a-Si:H). These variations of v_{ap}, v_{ag}, and v_{at} are observed to be essentially linear in the Si content of the films (see Fig. 9). A void component appears as Si is added, reaching a maximum value of 26% for $x=0.38$ before falling to zero for $x=0$ (a-Si:H).

The carbon concentrations in the films determined via the EMA, x(EMA), are in very good agreement with the values obtained from the Auger measurements, with two

TABLE II. Results of EMA for volume fractions of film components.

x[a]	x(EMA)[b]	v_{ap}[c]	v_{ag}[d]	v_{at}[e]	v_{void}[f]	x_{at}[g]
1.00	1.0(a-C:H)	0.67	0.17	0.16	0.00	1.00
0.96	0.96±0.01	0.68	0.15	0.17	0.00	0.90
0.84	0.83±0.03	0.52±0.04	0.12	0.27±0.03	0.09±0.04	0.65
0.68	0.68±0.04	0.31±0.08	0.11	0.42±0.04	0.16±0.05	0.48
0.57	0.54±0.04	0.25±0.10	0.05	0.52±0.04	0.18±0.08	0.38
0.38	0.38±0.02	0.03±0.03	0.00	0.71±0.02	0.26±0.04	0.365
	0.28±0.01	0.00±0.02	0.00	0.80	0.20	0.28
0.07	0.16±0.01	0.00	0.00	0.85±0.02	0.15±0.02	0.16
0.00	0.0(a-Si:H)	0.00	0.00	1.00	0.00	0.00

[a]Carbon fractional content of film determined from scanning Auger microprobe.
[b]Carbon fractional content of film determined using the EMA, see text.
[c]Volume fraction of amorphous polymeric component.
[d]Volume fraction of amorphous graphitic component.
[e]Volume fraction of amorphous tetrahedral component.
[f]Volume fraction of void component.
[g]Carbon fractional content of amorphous tetrahedral component.

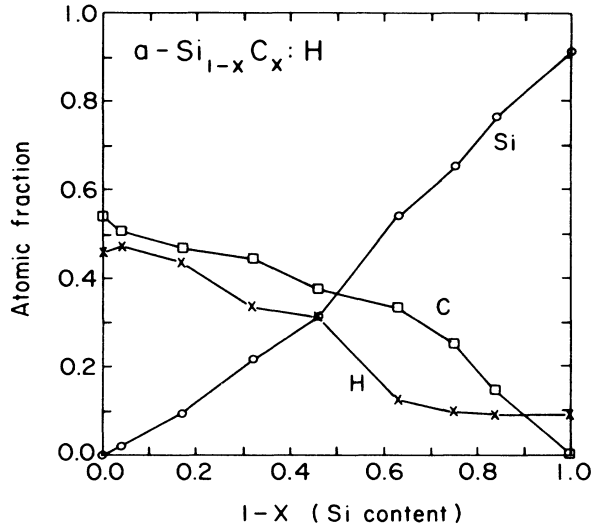

FIG. 10. Atomic fractions of the three elements present in these a-$Si_{1-x}C_x$:H films, as functions of $1-x$ (Si content).

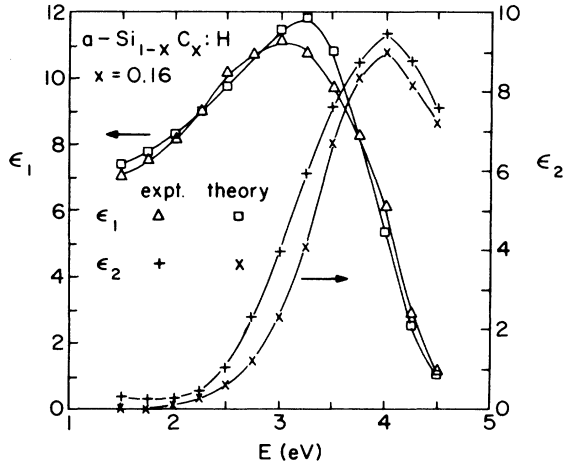

FIG. 12. ϵ_1 and ϵ_2 vs photon energy for a-$Si_{0.84}C_{0.16}$:H. Comparison between experiment and theoretical prediction of EMA for complete chemical ordering with homogeneous dispersion.

films requiring additional comment. An Auger analysis of the composition of the x(EMA)$=0.28$ film was not undertaken, so that no comparison is possible for this sample. In addition, the sample for which a carbon fraction of $x=0.07$ was determined via Auger was prepared under somewhat different discharge conditions (higher dc bias voltage on powered electrode) than the sample for which optical measurements were made and for which x(EMA)$=0.16$ was determined. The carbon content of the amorphous tetrahedral component, x_{at}, shows the expected decrease from $x_{at}=1.0$ for a-C:H to $x_{at}=0.0$ for a-Si:H, see Table II.

In addition to obtaining the volume fractions v_i for the various components in the films from the EMA, we can also obtain information about the fractional atomic concentrations of carbon, hydrogen, and silicon in the films by combining the EMA results for the v_i with the bonded hydrogen concentrations obtained from the ir measurements. For $x=0$ (a-Si:H) we found about 8 at.% H in the film and have used this for the hydrogen content of the amorphous tetrahedral component for all compositions $0 \leq x \leq 1$. For $x=1$ (a-C:H) we found 54 at.% H, which, when attributed to the amorphous polymeric component (a-CH_m) with volume fraction of 0.67, is equivalent to a stoichiometry of approximately $CH_{2.5}$ for this component. For consistency with our use of the smoothed polyethylene spectrum for the amorphous polymeric component, we have chosen instead to use CH_2 as its stoichiometry.

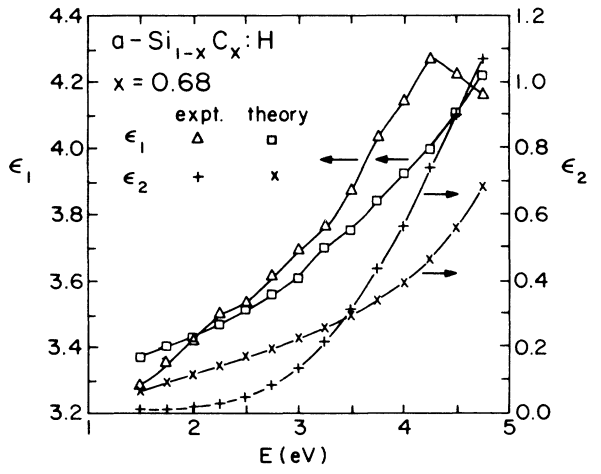

FIG. 11. ϵ_1 and ϵ_2 vs photon energy for a-$Si_{0.32}C_{0.68}$:H. Comparison between experiment and theoretical prediction of EMA for complete chemical ordering with homogeneous dispersion.

In Fig. 10 we show the resulting Si, C, and H fractions in the films as functions of the Si content (excluding hydrogen). For $x=1$, a-C:H, the film is found to have a composition corresponding to 54 at.% C and 46 at.% H, which is in reasonable agreement with our ir determination of (54 ± 14) at.% H. It is clear from Fig. 10 and our ir results that the C-rich films contain three to four times as much hydrogen as the Si-rich films. In Figs. 11 and 12 we show both the measured ϵ_1 and ϵ_2 and also the results of the EMA for ϵ_1 and ϵ_2, assuming complete chemical ordering with homogeneous dispersion, for the $x=0.68$ and $x=0.16$ samples, respectively.

IV. DISCUSSION

Film composition is a critical parameter for understanding and developing a model for the optical constants of these a-$Si_{1-x}C_x$:H alloy films. The carbon concentrations determined via Auger, x, and via the EMA, x(EMA), have been found to be in very good agreement with each other, to within ±0.03 (see Table I), thus strengthening the conclusions which we have reached based on the results of our EMA model.

In addition to quantitative agreement on composition, the Auger and optical results have also both been found to be sensitive to film inhomogeneity in that both gave evidence for an enhancement of the C concentration at the film-substrate interface in the Si-rich films. This initial C buildup may be due to an enhanced initial breakdown of C_2H_2 in the discharge relative to SiH_4.

Hydrogen also plays a crucial role in the properties of these films, and we have used our ir results along with the results of the EMA model to determine the atomic fractions of the three elements present in these films, Si, C, and H. These results, presented in Fig. 10 as functions of Si content $(1-x)$, indicate that the hydrogen atomic fraction decreases from about 0.5 for $x=1$ (a-C:H) to about 0.1 for $x=0$ (a-Si:H). The ir modes observed are consistent with a considerable amount of the hydrogen in the a-C:H film bonded in CH_2 and CH_3 groups. These ir results for the amount of H bonded and the presence of CH_2 and CH_3 groups in a-C:H are consistent with the presence of a significant amorphous polymeric component,[19,34] with composition given approximately by a-CH_2. In the a-Si:H film, most of the hydrogen is bonded in SiH_2 groups.

The observed increase in film density from 1.36 g/cm^3 for a-C:H to 2.07 g/cm^3 for a-Si:H is consistent with a decrease in the volume fraction of the low-density amorphous polymeric component and the incorporation of increasing amounts of Si into the higher density amorphous tetrahedral component as a-Si:H is approached. Our measured low value for the density of a-Si:H, 2.07 relative to 2.33 g/cm^3 for crystalline Si, results from the porous nature of the film, as evidenced by the predominance of dihydride, SiH_2, groups in the film as observed via ir. The use of Ar to dilute the SiH_4 in the glow-discharge deposition of a-Si:H, as we have employed, is known to result in the production of porous films.[35]

The optical constants n and k, ϵ_1 and ϵ_2 show a systematic variation with film composition from a-C:H ($x=1$) to a-Si:H ($x=0$). The index of refraction n is low for a-C:H, ~ 1.7, and increases as the Si concentration increases, see Fig. 2. This increase in n, which is consistent with the observations of previous workers,[5,13,36] can be attributed to the decrease in the average energy gap parameter E_g, which is related to n via the expression[37]

$$n^2-1=A(\hbar\omega_p/E_g)^2 , \tag{3}$$

where ω_p is the plasma frequency (proportional to the square root of the valence electron concentration in the film), and A is a constant. According to the Si- and C-centered tetrahedron model presented in the preceding paper,[21] E_g decreases from 13.62 to 4.76 eV as x decreases from 1 to 0 in the a-$Si_{1-x}C_x$:H alloy series (i.e, from a-C:H to a-Si:H). This decrease in E_g is also responsible for the increasing dispersion observed in n as the Si content increases from a-C:H to a-Si:H, see Fig. 2.

The imaginary part of the index k initially shows a small decrease, about 15% at 4.75 eV, as Si is added to a-C:H (see Fig. 3). This decrease in absorption results from the replacement of strongly absorbing graphitic C—C bonds by Si—C bonds which absorb at higher energies. At higher Si concentrations, k increases again as Si—C bonds are replaced by Si—Si bonds which absorb at lower energies. The dependences of $\epsilon_1=n^2-k^2$ and $\epsilon_2=2nk$ on x (see Figs. 4 and 5) essentially reflect the previously discussed dependences of n and k on x.

Comparisons between the ϵ_1 and ϵ_2 spectra predicted by the EMA and the measured spectra are presented in Figs. 7, 8, 11, and 12. In Figs. 7 and 8 the measured ϵ_1 and ϵ_2 spectra for the film with a carbon fraction of 0.38 are compared with three separate predictions[21] of the EMA, each corresponding to a different form of chemical ordering between the carbon and silicon atoms in the amorphous tetrahedral component: (1) complete chemical ordering with homogeneous dispersion, (2) complete chemical ordering with phase separation, and (3) no chemical ordering. The latter two predictions both yield spectra with peaks in ϵ_1 and ϵ_2 at energies which are too low by at least 0.5 eV when compared to the measured ϵ_1 and ϵ_2. This stronger absorption at lower energies for predictions (2) and (3) can be attributed to the presence of highly absorbing Si-Si_4 tetrahedra in the amorphous tetrahedral component. In particular, for this film with a carbon fraction of $x_{at}=0.365$ in the amorphous tetrahedral component (see Table II), the fraction of all tetrahedra which are Si-Si_4 tetrahedra is only 0.021 for complete chemical ordering with homogeneous dispersion, 0.103 for no chemical ordering, and 0.270 for complete chemical ordering with phase separation.[21] It is clear that the measured spectra are quite consistent with the low fraction of Si-Si_4 tetrahedra as given by complete chemical with homogeneous dispersion.

Figures 11 and 12 show comparisons between the measured ϵ_1 and ϵ_2 for films with carbon fractions of 0.68 and 0.16, respectively, and EMA predictions for the case of complete chemical ordering with homogeneous dispersion in the amorphous tetrahedral component. For the C-rich sample with $x=0.68$, the agreement between experiment and the EMA prediction is good for ϵ_1 but not as satisfactory for ϵ_2. The higher ϵ_2 at low energies of the predicted spectrum as compared to that of the measured spectrum is due to the amorphous graphitic component in the EMA with a volume fraction $v_{ag}=0.11$ for this film (see Table II). Clearly the spectrum we use in the EMA for amorphous graphitic component is too highly absorbing at low energies. This was also observed previously[19] in the case of an a-C:H film and remains an area for improvement in the EMA. In Fig. 12 the measured spectra for ϵ_1 and ϵ_2 are both seen to be in very good agreement with the predictions of the EMA. The spectra of films with such a low carbon content of only 0.16 are not, however, very sensitive to the degree or type of chemical ordering present in the film.

The addition of Si to a-C:H leads to an initial increase in $E_{\rm opt}$, and from Tables I and II and Fig. 13, where $E_{\rm opt}$ is plotted as a function of the volume fraction of the amorphous graphitic component v_{ag}, it can be seen this increase in $E_{\rm opt}$ is associated with a decrease in v_{ag}. Also included in Fig. 13 are previous results for an annealed a-C:H film,[19] where it was found that $E_{\rm opt}$ goes to zero when v_{ag} reaches a value of 0.75. The increase in $E_{\rm opt}$ as Si is added to a-C:H reaches a maximum value of 2.68 eV for a Si fraction of 0.32, in good agreement with the re-

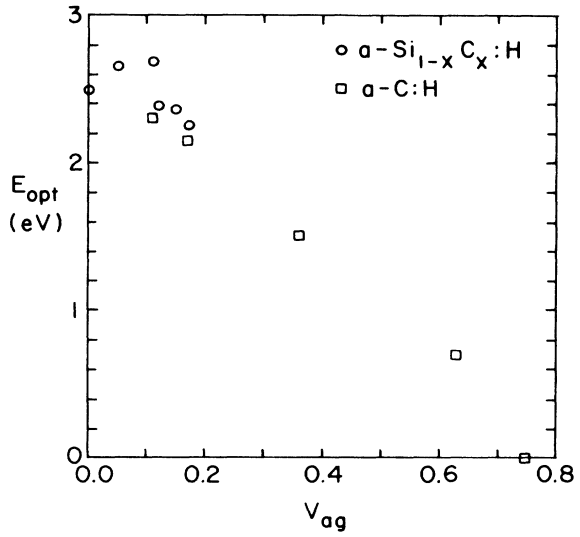

FIG. 13. Optical energy gap E_{opt} vs volume fraction v_{ag} of amorphous graphitic component for two sets of samples: a-$Si_{1-x}C_x$:H (this work) and a-C:H (Ref. 19).

sults of other workers.[1,5,24] E_{opt} then decreases as the Si concentration increases further. This decrease in E_{opt} for Si fractions greater than 0.32 starts at the point where the amorphous tetrahedral component becomes Si-rich (i.e., $x_{at} < 0.5$; see Table II), and hence, even for the case of complete chemical ordering, Si—Si bonds must be present in the film. Since Si—Si bonds absorb at lower energies than either Si—C or tetrahedral C—C bonds, their presence in the films shifts the absorption edge to lower energies, leading to lower values of E_{opt} for a Si fraction greater than 0.32.

It is important to note that the observed increase in E_{opt} from 2.24 to 2.68 eV as the Si fraction increases from 0 to 0.32 is associated with only very small changes in absorption, i.e., small decreases in k and ϵ_2, see Figs. 3 and 5. In addition, the film with the highest E_{opt} of 2.68 eV actually has higher absorption for all energies in the measured range, 1.5—4.75 eV, than does the film with Si fraction of 0.16 which has $E_{opt} = 2.38$ eV. The higher E_{opt} for a Si fraction of 0.32 clearly results from a sharper absorption edge rather than from lower overall optical absorption. We conclude that the increase in E_{opt} with Si concentration results not from shifts of the band edges (E_c or E_v), but from changes in the regions of the localized tail states where the energy levels of the localized π electrons associated with the amorphous graphitic component are located. These localized tail state bands will become narrower as Si is added and v_{ag} decreases. This picture is consistent with the observed increase in the slope parameters B_1 and B_T (see Table I) with increasing Si concentration.

E_{opt} also increases as C is added to a-Si:H, which can be understood as due to the replacement of weaker Si—Si bonds by stronger Si—C bonds in the amorphous tetrahedral component. Ultimately, as the C content increases further, graphitic C—C bonds appear in the film and E_{opt} begins to decrease. The slope parameters B_1 [from $E(\epsilon_2)^{1/2}$ versus E] and B_T (from $\sqrt{\alpha E}$ versus E) both decrease (see Table I) as C is added to a-Si:H, signaling increasing widths for the bands of localized tail states. This increase in width arises from increased compositional disorder in the films. Si—C bonds are much shorter (1.88 Å) than Si—Si bonds (2.35 Å), and so bond-angle distortions will be enhanced in a-$Si_{1-x}C_x$:H as compositional disorder is added to the topological disorder already present in a-Si:H.[38] Note that the low values of B_1 and B_T for a-Si:H result from the predominantly dihydride (SiH_2) bonding for hydrogen in this film.

Additional confirmation for the existence of complete chemical ordering with homogeneous dispersion in the films comes from the observed experimental variation of E_{opt} with carbon fraction x, shown in Fig. 14 along with the predictions[21] of the EMA assuming the amorphous tetrahedral component to be the only component present in the films. The observed values of E_{opt} up to $x = 0.4$ are in much better agreement with the predicted values assuming complete chemical ordering with homogeneous dispersion than with the predicted values assuming either phase separation or no chemical order. Deviations between the model and experiment begin for $x > 0.4$, the carbon concentration above which the amorphous graphitic component begins to appear in the film (see Table II and Fig. 9). Again, it is the appearance of this amorphous graphitic component which limits E_{opt} as the carbon fraction x increases in the films.

Our use of the EMA to describe the optical spectra of these a-$Si_{1-x}C_x$:H films has provided useful information on the variations of the volume fractions of the four proposed components (amorphous polymeric, amorphous graphitic, amorphous tetrahedral, and void) as functions

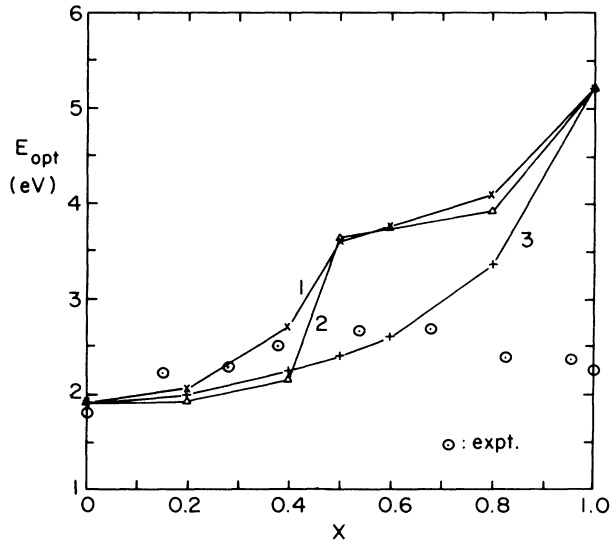

FIG. 14. Optical energy gap E_{opt} vs carbon fraction x both for experiment and theory. Curve 1: prediction for complete chemical order with homogeneous dispersion; curve 2: complete chemical order with phase separation; curve 3: no chemical order.

of film composition. Although clearly an oversimplification for the structure of these films, our model is a successful first approximation to the local bonding and has provided a useful framework for understanding the properties of this technologically important alloy series. Improvements to the model should focus on a better treatment of the optical absorption due to the localized π-like electrons associated with the amorphous graphitic component and explicit calculations of the effects of hydrogen incorporation on the optical response of the amorphous polymeric and tetrahedral components.

There exists additional experimental evidence supporting our use of amorphous polymeric, graphitic, and tetrahedral components in the EMA. ir studies,[39–41] including our own results, have indicated that the majority of the hydrogen in these films is bonded to C, as opposed to Si, thus supporting the use of an amorphous polymeric component with approximate composition CH_2 and an amorphous tetrahedral component with a much lower H content, ~ 10 at. %. We note here that an additional improvement to our model would be to allow the hydrogen content of the amorphous tetrahedral component to increase as the C content of this component increases. NMR studies[42] also point to the existence of two hydrogen-containing phases in a-$Si_{1-x}C_x$:H alloys: heavily hydrogenated C clusters (the amorphous polymeric component) and a weakly hydrogenated a-Si lattice (the amorphous tetrahedral component).

The EMA indicates that a void component appears in these a-$Si_{1-x}C_x$:H films from the Si-rich end as C is added to a-Si:H and also from the C-rich end as Si is added to a-C:H. The increased compositional disorder[38] in the films as a result of alloying leads to the generation of voids due to the inability of the various components to fit together perfectly. The maximum void volume fraction of 0.26 occurs for a C fraction of 0.38, the composition at which the volume fraction of the amorphous polymeric component drops to a very low value (0.03). The amorphous polymeric component is thus proposed to be effective in helping to relax the amorphous network so that the components fit together better, with less of a tendency for the presence of voids.

Relaxation of the amorphous network by the hydrogen-containing amorphous polymeric component can also be understood in terms of the average coordination number $\overline{Z}$ for a particular alloy, e.g., a-$Si_wC_yH_z$. Here $w+y+z=1$ and the carbon fraction can be written as the sum of tetrahedral (y_t) and graphitic (y_g) parts, i.e., $y=y_t+y_g$. With this notation we have $\overline{Z}=4-y_g-3z$. Using our results for the volume fractions (Table II) and atomic fractions (Fig. 10), we calculate $\overline{Z}=2.4\pm0.2$ for a-C:H and $\overline{Z}=3.75\pm0.1$ for a-Si:H, with $\overline{Z}$ increasing smoothly between these two limits as the Si content increases. This result for a-C:H is very close to the value $\overline{Z}=\sqrt{6}=2.45$ given by Phillips[43] as the average coordination number for an alloy in which all bond-length and bond-angle constraints are satisfied, thereby reducing the strain in the alloy.

From our use of the EMA for the ϵ_1 and ϵ_2 spectra we have clear evidence for a strong tendency for homogeneous chemical ordering of the C and Si atoms for our Si-rich samples where the amorphous tetrahedral component is dominant. The situation on the C-rich side of the alloy series is complicated by the presence of the amorphous polymeric and graphitic components. Still, we do see a tendency toward at least partial chemical ordering both from our ϵ_1 and ϵ_2 results. The driving force for chemical ordering, i.e., the presence of the maximum number possible of Si—C bonds in a film, is likely to be a lowering of the free energy. The Si—C bond is more stable than the average of the Si—Si and C—C bonds.[44] In a particular a-$Si_{1-x}C_x$:H sample, however, the degree of chemical ordering present will be critically dependent on the deposition conditions.

In this regard, a variety of different claims have been made previously concerning the existence of chemical ordering in amorphous silicon-carbon alloy films. Raman studies[45] have shown that chemical ordering is not complete in some Si-rich alloy films as C—C bonds have been observed. A careful analysis[3] of the ir spectra of a-$Si_{1-x}C_x$:H films has led to the conclusion that the compositional dependences of the Si—H, C—H, and Si—C modes are all consistent with no chemical ordering, i.e., a random distribution of C and Si atoms. X-ray photoemission spectroscopy results[4] have also been stated to be consistent with no chemical ordering. However, the observed constancy of the energy of the C $1s$ core level in Si-rich alloys is consistent with chemical ordering, i.e., C atoms bonded only to four Si atoms.[4,46] A recent study[8] using electron energy-loss spectroscopy and electron diffraction on an a-$Si_{0.68}C_{0.32}$:H film has led to the conclusion that C atoms tend to be surrounded by four Si atoms, thus indicating that chemical ordering is present in the film.

Some very recent experimental studies[47,48] of a-$Si_{1-x}C_x$:H alloy films using x-ray diffraction and electron energy-loss spectroscopy have also provided evidence for the domination of the tetrahedral component in Si-rich films, with the appearance of graphitic C—C bonding arising as the C content increases.

In addition to providing results for the variations of the volume fractions of the various components present in these a-$Si_{1-x}C_x$:H films with composition and for the existence of chemical ordering of the Si and C atoms, the use of the EMA has also shown that the C- and Si-centered tetrahedron model[21] successfully describes the optical response of the amorphous tetrahedral component. Thus, this model presented in the preceding article has been shown to be a useful method for calculating the ϵ_1 and ϵ_2 spectra of disordered tetrahedral materials. A remaining problem is to directly include in the tetrahedron model the effect of hydrogen on the optical response.

V. CONCLUSIONS

We have undertaken an experimental determination of the optical constants (n, k, ϵ_1, and ϵ_2) for the entire a-$Si_{1-x}C_x$:H alloy series, from a-C:H to a-Si:H. We have successfully employed the EMA based on four components (amorphous polymeric, graphitic, tetrahedral, and void) to model the measured ϵ_1 and ϵ_2 spectra. The resulting volume fractions for these four components show sys-

tematic variations with film composition and provide a very useful framework for understanding the properties of this technologically important alloy series. In particular, the use of the EMA has provided a convincing demonstration that it is the appearance of the amorphous graphitic component which limits the optical energy gap E_{opt} as the carbon content of the film increases. The use of a Si- and C-centered tetrahedron model (presented in the preceding paper) has been shown to successfully represent the optical response of the amorphous tetrahedral component. Our experimental results for ϵ_1 and ϵ_2 are consistent with complete homogeneous chemical ordering in the amorphous tetrahedral component for Si-rich films, in which every C atom is surrounded by four Si atoms. Although the question of chemical ordering is complicated in the C-rich films due to the added complication of the presence of amorphous polymeric and graphitic components, there still appears to be a tendency for at least partial chemical ordering. We can clearly exclude chemical ordering with phase separation in these as-deposited a-$Si_{1-x}C_x$:H films.

ACKNOWLEDGMENTS

We wish to thank M. H. Brodsky, I. Haller, and J. Nocero of the IBM Thomas J. Watson Research Center (Yorktown Heights, NY) and also A. Woodward of the City College, for taking the ir absorption spectra. This research was supported by the U. S. Department of Energy at the City College under Grant No. DE-FG02-84ER45168-A000 and at Brookhaven National Laboratory under Contract No. DE-AC02-76CH00016. The research of K.M., F.W.S., and D.K.B. was supported by the U. S. Department of Energy under Grant No. DE-FG02-84ER45168-A000. The research of R.C. was performed under the auspices of the U. S. Department of Energy (Division of Materials Sciences, Office of Basic Energy Sciences), under Contract No. DE-AC02-76CH00016.

*On leave from Department of Physics, Utkal University, Bhubaneswar 751 004, Orissa, India.

[1]D. A. Anderson and W. E. Spear, Philos, Mag. **35**, 1 (1977).

[2]T. Shimada, Y. Katayama, and K. F. Komatsubara, J. Appl. Phys. **50**, 5530 (1979).

[3]H. Wieder, M. Cardona, and C. R. Guarnieri, Phys. Status Solidi B **92**, 99 (1979).

[4]Y. Katayama, K. Usami, and T. Shimada, Philos. Mag. B **43**, 283 (1981).

[5]R. S. Sussmann and R. Ogden, Philos. Mag. B **44**, 137 (1981).

[6]Y. Katayama, T. Shimada, and K. Usami, Phys. Rev. Lett. **46**, 1146 (1981).

[7]N. Saito, T. Yamada, T. Yamaguchi, I. Nakaaki, and N. Tanaka, Philos. Mag. B **52**, 987 (1985).

[8]J. Tafto and F. J. Kampas, Appl. Phys. Lett. **46**, 949 (1985).

[9]A. H. Mahan, B. von Roedern, D. L. Williamson, and A. Madan, J. Appl. Phys. **57**, 2717 (1985).

[10]K. Mui, D. K. Basa, and F. W. Smith, J. Appl. Phys. **59**, 582 (1986).

[11]Y. Tawada, H. Okamoto, and Y. Hamakawa, Appl. Phys. Lett. **39**, 237 (1981).

[12]Y. Tawada, K. Tsuge, M. Kondo, H. Okamoto, and Y. Hamakawa, J. Appl. Phys. **53**, 5273 (1982).

[13]D. R. McKenzie, N. Savvides, D. R. Mills, R. C. McPhedran, and L. C. Botten, Solar Energy Mater. **9**, 113 (1983).

[14]M. H. Brodsky, Thin Solid Films **50**, 57 (1978).

[15]D. A. Anderson, Philos. Mag. **35**, 17 (1977).

[16]B. Meyerson and F. W. Smith, J. Non-Cryst. Solids **35/36**, 435 (1980).

[17]L. P. Andersson, Thin Solid Films **86**, 193 (1981).

[18]A. Bubenzer, B. Dischler, and A. Nyaiesh, Thin Solid Films **91**, 81 (1982).

[19]F. W. Smith, J. Appl. Phys. **55**, 764 (1984).

[20]B. Meyerson and F. W. Smith, Solid State Commun. **34**, 531 (1980).

[21]K. Mui and F. W. Smith, preceding paper, Phys. Rev. B **35**, 8080 (1987).

[22]D. E. Aspnes and J. B. Theeten, J. Appl. Phys. **50**, 4928 (1979).

[23]D. A. G. Bruggemann, Ann. Phys. (Leipzig) **24**, 636 (1935).

[24]J. Bullot, M. Gauthier, M. Schmidt, Y. Catherine, and A. Zamouche, Philos. Mag. B **49**, 489 (1984).

[25]L. E. Davis, N. C. MacDonald, P. W. Palmberg, G. E. Riach, and R. E. Weber, *Handbook of Auger Electron Spectroscopy,* 2nd ed. (Physical Electronics Division, Perkin-Elmer Corporation, Eden Prairie, MN, 1976).

[26]F. Fujimoto, A. Ootsuka, K. Komaki, Y. Iwata, I. Yamane, H. Hamashita, Y. Hashimoto, Y. Tawada, K. Nishimura, H. Okamoto, and Y. Hamakawa, Jpn. J. Appl. Phys. **23**, 810 (1984).

[27]K. Nakazawa, S. Ueda, M. Kumeda, A. Morimoto, and T. Shimizu, Jpn. J. Appl. Phys. **21**, L176 (1982).

[28]C. J. Fang, L. Ley, H. R. Shanks, K. J. Gruntz, and M. Cardona, Phys. Rev. B **22**, 6140 (1980).

[29]O. S. Heavens, *Optical Properties in Thin Solid Films* (Academic, New York, 1955), Chap. 4.

[30]C. L. Nagendra and G. K. M. Thutupalli, Vacuum **31**, 141 (1981).

[31]J. Tauc, R. Grigorovici, and A. Vancu, Phys. Status Solidi **15**, 627 (1966).

[32]H. R. Philipp, J. Phys. Chem. Solids **32**, 1935 (1971); J. Electrochem. Soc. **120**, 295 (1973).

[33]L. R. Painter, E. T. Arakawa, M. W. Williams, and J. C. Ashley, Radiat. Res. **83**, 1 (1980).

[34]D. R. McKenzie, L. C. Botten, and R. C. McPhedran, Phys. Rev. Lett. **51**, 280 (1983).

[35]J. C. Knights, R. A. Lujan, M. P. Rosenblum, R. A. Street, D. K. Bieglesen, and J. A. Reimer, Appl. Phys. Lett. **38**, 331 (1981).

[36]Y. Catherine and G. Turban, Thin Solid Films **60**, 193 (1979).

[37]J. C. Phillips, *Bonds and Bands in Semiconductors* (Academic, New York, 1973), p. 35.

[38]A. Skumanich, A. Frova, and N. M. Amer. Solid State Commun. **54**, 597 (1985); F. Boulitrop, J. Bullot, M. Gauthier, M. P. Schmidt, and Y. Catherine, *ibid.* **54**, 107 (1985).

[39]A. Guivarc'h, J. Richard, M. Le Contellec, E. Ligeon, and J. Fontenille, J. Appl. Phys. **51**, 2167 (1980).

[40]Y. Catherine, A. Zamouche, J. Bullot, and M. Gauthier, Thin

Solid Films **109**, 145 (1983).
[41]J. Saraie, Y. Fujii, M. Yoshimoto, K. Yamazoe, and H. Matsunami, Thin Solid Films **117**, 59 (1984).
[42]J. A. Reimer, R. W. Vaughan, J. C. Knights, and R. A. Lujan, J. Vac. Sci. Technol. **19**, 53 (1981).
[43]J. C. Phillips, J. Non-Cryst. Solids **34**, 153 (1979).
[44]J. L. Martins and A. Zunger, Phys. Rev. Lett. **56**, 1400 (1986).
[45]M. Gorman and S. Solin, Solid State Commun. **15**, 761 (1974).
[46]W. Y. Lee, J. Appl. Phys. **51**, 3365 (1980).
[47]D. R. McKenzie, S. D. Berger, and L. M. Brown, Solid State Commun. **59**, 325 (1986).
[48]A. Sproul, D. R. McKenzie, and D. J. H. Cockayne, Philos. Mag. B **54**, 113 (1986).